

Photodynamic Therapy Creates Fluence Rate-dependent Gradients in the Intratumoral Spatial Distribution of Oxygen¹

Theresa M. Busch,² E. Paul Wileyto, Micheal J. Emanuele, Fabio Del Piero, Laura Marconato, Eli Glatstein, and Cameron J. Koch

Department of Radiation Oncology [T. M. B., M. J. E., E. G., C. J. K.] and Tobacco Use Research Center [E. P. W.], School of Medicine, University of Pennsylvania, Philadelphia, Pennsylvania 19104-6072, and Department of Pathobiology, School of Veterinary Medicine, University of Pennsylvania, Kennett Square, Pennsylvania 19348 [F. D. P., L. M.]

ABSTRACT

In photodynamic therapy (PDT), treatment efficacy may be reduced by the presence of pre-existing tumor hypoxia or by oxygen depletion during the therapy. Tumor oxygenation during PDT has been measured with needle electrodes, but the intratumoral distribution of this oxygen is not known. In the present study, the spatial distribution of hypoxia during PDT was quantified using the hypoxia-labeling marker EF3. Mice bearing radiation-induced fibrosarcoma tumors were treated with Photofrin-mediated PDT to a total dose of 135 J/cm², delivered at a fluence rate of either 75 mW/cm² or 38 mW/cm². PDT-created hypoxia at each fluence rate was labeled by exposing tumors to EF3 (52 mg/kg) during the period of illumination. Cryosectioning, immunohistochemistry, and fluorescence microscopy were carried out to quantify EF3 binding as a function of distance to the nearest perfused blood vessels in sections cut from within the superficial (light-adjacent) 600 μ m or the deep (light-distant) 600 μ m of tumors (5–6 mm in diameter, \sim 3 mm in depth). In both superficial and deep sections, PDT at 75 mW/cm² resulted in the development of significant gradients in tumor hypoxia as a function of distance to a perfused blood vessel. Furthermore, significant hypoxia was detected even in vascular-adjacent tissue. These effects were associated with a significant decrease in the percentage of perfused vessels and a significant increase in the median distance of a cell to the nearest perfused blood vessel. In contrast, during PDT at 38 mW/cm², sections from deep tumor levels demonstrated only insignificant increases in the rise in hypoxia as a function of distance to a perfused vessel and in the level of hypoxia in vascular-adjacent tissue. No effects on tumor perfusion were detected during PDT at 38 mW/cm². Overall, these results demonstrate that spatially dependent depletion of oxygen can occur during PDT as a function of the fluence rate and that PDT can create significant hypoxia in even tissue adjacent to perfused blood vessels.

INTRODUCTION

The oxygen dependence of PDT³ has been well established (1, 2). PDT involves the administration of a photosensitizer that accumulates in malignant tissue and the subsequent illumination of this tissue with visible light of a specific, photosensitizer-dependent wavelength. The light-excited photosensitizer interacts with ground state oxygen, leading to the formation of tissue-damaging reactive oxygen species. Oxygen is consumed by this process, potentially resulting in the development of tissue hypoxia during PDT itself (3). Additionally contributing to hypoxia during PDT can be the development of blood vessel damage and accompanying reductions in tumor perfusion (4). Thus, PDT outcome is affected by not only pre-existing tumor hypoxia (5) but also by any hypoxia created during illumination by PDT photochemistry (6).

Several light delivery techniques have been found to facilitate the conservation of tumor oxygenation during PDT. Microelectrode measurements of tumor pO₂ show that fractionated PDT enables cycling consumption and replenishment of tumor oxygenation (7). Similarly, needle electrode measurements indicate improved maintenance of tumor oxygenation as the fluence rate of PDT is lowered (6). In many of these types of measurements, substantial intratumoral heterogeneity in oxygenation during PDT is observed as a function of probe placement (7, 8). Such results are not unexpected; metabolism-created radial gradients of tissue oxygen, *i.e.*, the decline in oxygen concentration at increased distances from a blood vessel, are known to occur (9, 10), and mathematical models predict that PDT may amplify the severity of such gradients (3, 11). Van Geel *et al.* (12) observed an inverse relationship between areas of hypoxia marker binding and vascular perfusion in tumors after treatment with PDT. However, the spatial quantification of microscopic oxygen gradients during PDT has yet to be accomplished.

The present article describes a novel protocol using the hypoxia marker EF3 to quantify intratumoral gradients in oxygen during PDT. EF3 binds nonreversibly to hypoxic cells as an inverse function of the oxygen concentration (13). Image analysis of EF3 binding in PDT-treated murine tumors revealed that PDT created gradients of increasing hypoxia at increased distance to the nearest perfused blood vessel. In sections collected from both the superficial and deep side of RIF tumors (approximately 5–7 mm diameter, \sim 3 mm depth), Photofrin PDT at 75 mW/cm², 135 J/cm² created significant hypoxia even in close proximity to the blood supply, *i.e.*, in vascular-adjacent tissue. In contrast, during PDT at 38 mW/cm², deep tumor depths exhibited EF3 binding in vascular-adjacent tissue, which was not significantly different from control levels. These findings demonstrate *in vivo* that spatially dependent depletion of tumor oxygenation can occur during PDT as a function of fluence rate. Furthermore, PDT can create hypoxia even in close proximity to the blood vessels.

MATERIALS AND METHODS

PDT and EF3 Administration. RIF tumors were propagated on the shoulders of C3H mice (Taconic, Germantown, NY) by the intradermal injection of 3×10^5 cells (13). Animals were treated \sim 1 week later when tumors were a size of 5–7 mm in diameter and \sim 3 mm in depth. The photosensitizer Photofrin (Axcan Pharma Inc., Mont-Saint-Hilaire, Quebec, Canada) was administered via tail vein at 5 mg/kg at \sim 24 h before illumination. The laser system consisted of a KTP Yag pumped dye module (Laserscope, San Jose, CA) tuned to produce 630 nm of light. Light was delivered to a 1-cm diameter treatment field through microlens-tipped fibers (CardioFocus, Norton, MA), and the power density was measured with a power meter (Coherent, Auburn, CA). Laser output was adjusted to produce a fluence rate of 75 or 38 mW/cm², as indicated in the text. Treatment was to a total fluence of 135 J/cm², *i.e.*, 30 min at 75 mW/cm² and 60 min at 38 mW/cm². To label hypoxia during PDT, EF3 (synthesized by Dr. Bill Dolbier, University of Florida, Gainesville, FL; Ref. 13) was injected via tail vein at 52 mg/kg within 5 min before PDT was begun. Then mice were anesthetized (ketamine/xylazine at 150/10 mg/kg *i.p.*), and PDT was carried out. At 1.5 min before the completion of PDT, without removing the mice from the laser, Hoechst 33342 (Sigma, St. Louis, MO) was

Received 5/17/02; accepted 10/16/02.

The costs of publication of this article were defrayed in part by the payment of page charges. This article must therefore be hereby marked *advertisement* in accordance with 18 U.S.C. Section 1734 solely to indicate this fact.

¹ Supported by NIH RO1 Grant CA85831 and PO1 Grant CA87971.

² To whom requests for reprints should be addressed, at Department of Radiation Oncology, University of Pennsylvania, B13 Anatomy Chemistry Building, 3620 Hamilton Walk, Philadelphia, PA 19104-6072.

³ The abbreviations used are: PDT, photodynamic therapy; EF3, 2-(2-nitroimidazol-1[H]-yl)-N-(3,3,3-trifluoropropyl)acetamide; PF, paraformaldehyde; RIF, radiation-induced fibrosarcoma; CI, confidence interval.

injected via the orbital plexus at 30 mg/kg to label the cells around perfused blood vessels. Immediately on the completion of PDT, the tumor was excised, coated in Tissue-Tek OCT compound, and frozen on a dry-ice cooled aluminum plate. Controls included animals exposed only to EF3 for 30 min (marker only); animals exposed to Photofrin for 24 h and EF3 for 30 min (Photofrin and marker); and animals exposed to EF3 during illumination at 38 or 75 mW/cm² but not to Photofrin (light and marker).

Immunohistochemistry and Fluorescence Microscopy. Cryosectioning, immunohistochemistry, and fluorescence microscopy for EF3 were performed as described previously (13). Briefly, sections (14- μ m thickness) were cut parallel to the skin surface, *i.e.*, perpendicular to the light path for PDT. They were fixed with 4% PF, rinsed in Dulbecco's PBS (Sigma), and blocked in PBS containing 0.3% Tween 20 and 1.5% albumin, plus 20% nonfat milk and 5% normal mouse serum. Antibody staining for EF3 was performed for 4.5–5 h using a monoclonal antibody (ELK5-A8) conjugated to the fluorochrome Cy5 (Amersham Life Sciences, Arlington Heights, IL). Slides were rinsed in PBS containing 0.3% Tween 20 and PBS without Tween 20, and then stored in 1% PF. To analyze the spatial relationship between hypoxia and blood vessel distribution, some sections were stained for both EF3 and CD31. CD31 staining involved a 1.5-h incubation in primary antibody (rat antihuman CD31; PharMingen, San Diego, CA) and a 45-min incubation in secondary antibody (Cy5-conjugated mouse antirat IgG; Jackson ImmunoResearch, West Grove, PA). Both antibodies were diluted 1:100 in antibody carrier (14). CD31 staining was fixed by a 20-min incubation in 4% PF, then staining for EF3 was done as normal.

Fluorescence microscopy (LabPhot microscope with a 100-W high pressure mercury arc lamp and Photometrics Quantix CCD digital camera) was carried out to photograph a 2.16×1.44 mm area of each section. This was accomplished by creating a 2×2 mosaic of four adjacent $\times 10$ image fields consisting of 400×600 pixels each (1 pixel = 1.8 μ m). Sections were photographed for Hoechst-perfused blood vessels, EF3 binding (Cy3 label, excitation 550 nm, emission 570 nm) and CD31 staining (Cy5 label, excitation 649 nm, emission 670 nm). After photography of perfusion, slides were flooded with a solution of Hoechst 33342 (20 μ M in PBS) to label cell nuclei, and tissue placement was determined from a second image of Hoechst fluorescence. At the beginning and conclusion of each camera session, an image of hemacytometer-loaded calibration dye (Cy3 in 1% PF) was taken. The ratio of the exposure time to the mean fluorescence intensity of the calibration image ($\times 1000$) was used to correct the fluorescence intensities of experimental images (based on their exposure time) for day-to-day variations in the lamp intensity. Background fluorescence, determined from the lowest value on an image, was subtracted from each image. Staining controls for EF3 included sections receiving no antibody and sections receiving competed EF3 antibody (14). Staining controls for CD31 included sections receiving CD31 secondary antibody but not the primary antibody. All of the controls demonstrated low to negligible staining. The tumor areas studied were found to be free of microscopical necrosis as assessed by a veterinarian pathologist.

Image Analysis for EF3 Binding versus Distance to a Blood Vessel. Bitmap images (masks) were used to identify the parameters of interest during processing and analysis (15). Two types of masks were made: a feature mask and an alignment mask. Feature masks highlighted the feature of interest in that particular image, whereas alignment masks highlighted a feature common to all of the photos for a given section, *e.g.*, a hole in the tissue, to provide a reference point for alignment. Masks were created in Adobe PhotoShop (Adobe Systems Inc., San Jose, CA) by applying a series of functions and filters to the raw images. Alignment masks were made by applying the equalize function, followed by thresholding to highlight the hole or other feature common to all of the images. A tissue feature mask was created from the image of Hoechst-flooded tissue by applying an equalize function to brighten the image, the PhotoShop maximize and median filters to spread the nuclear-localized Hoechst fluorescence over the approximate diameter of a cell, and then thresholding. A feature mask of perfusion was made from the image of Hoechst-perfused blood vessels by applying the auto levels function to enhance contrast and thresholding. Similarly, a feature mask of CD31 was created using the auto levels and thresholding functions.

Images were processed and analyzed using a program written in the Matlab programming language (The Mathworks, Inc., Natick, MA). In the first step of image processing, images were aligned. The tissue feature mask was used as a base, and all of the other images were shifted in x and y coordinates until

landmarks on the alignment masks were aligned. Images were cropped to maintain the largest area common to all.

Sampling was performed by digitally superimposing a grid over the raw EF3 data. At the intersection of every 5th column and 5th row, *i.e.*, every 9 μ m, the pixel coordinates were checked against those pixels identified as containing tissue in the tissue feature mask. At tissue-containing points, the intensity value of EF3 was recorded as well as the distance traveled from that point to pixels identified as containing a perfused blood vessel. The latter was determined in Matlab by the creation of an overlay of the perfused feature mask and the CD31 feature mask. In the final data set, the shortest distance traveled in any direction from a tissue-containing coordinate to a perfused blood vessel was saved. Typically 11,000–13,000 data points were calculated from each image.

All of the data were sorted in Excel (Microsoft Corporation, Redmond, WA) based on distance (in pixels), and then EF3 intensity values were averaged within bins of 5 pixels each. Distances in pixels were converted to μ m based on the photography-determined scale of 1.8 μ m/pixel. Plots were created in SigmaPlot (SPSS Inc., Chicago, IL) and fit with a four-parameter sigmoid curve. The distance over which EF3 binding was plotted was a function of that required for binding levels to reach a plateau. This distance varied among images but was typically between 117 and 252 μ m. No significant effect of treatment on the distance required to reach a plateau in hypoxia could be detected.

The reported value for EF3 binding in vascular-adjacent tissue was the y intercept (y_0), which was calculated based on the sigmoid curve fit [$y = d + a / (1 + e^{-(b-x)})$]. The distant-dependent rise in EF3 binding was the a value resulting from this curve fit. No significant difference in the y_0 values or the a values was found among the controls exposed to EF3 for 30 min (marker only, Photofrin and marker, and light and marker). Therefore, these controls were combined for graphing purposes and for statistical tests comparing them to PDT at 75 mW/cm². Controls for PDT at 38 mW/cm² consisted of tumors treated with light and marker at the same fluence and fluence rate (1-h exposure).

Image Analysis for Blood Vessel Distribution and Perfusion. The frequency distribution of distances from a cell to the nearest perfused blood vessel was determined based on the same coordinate grid used to calculate EF3 binding distributions. At each tissue-containing point on this grid, the distance to the nearest perfused blood vessel was calculated. In Excel, data were sorted based on distance, and a lookup function was used to determine the distance of a cell to the nearest perfused blood vessel at designated percentages of the total points (cells) evaluated.

To evaluate the perfused fraction of blood vessels, feature masks of CD31, Hoechst-perfused blood vessels, and the entire tissue area were aligned in Matlab, and an overlay was created. For this analysis, the feature mask of Hoechst-perfused vessels was modified from that used for the EF3 spatial analysis. To reduce the granular nature of the latter, a Gaussian blur function was applied just before thresholding. The aligned, overlaid image was opened in Adobe PhotoShop, and the tissue feature mask was used to determine tissue-containing areas. Within these areas, the number of CD31-stained pixels versus the number of both CD31- and Hoechst-stained pixels was determined. The perfused percentage was calculated as $100 \times (\text{number of perfused CD31-stained pixels}) / (\text{number of CD31-stained pixels})$.

EF3 Binding in Euthanized (Hypoxic) Animals. Euthanized animal controls were used to study the access of EF3 to tumors under control and PDT-treated conditions. In these studies, animals were administered EF3 (52 mg/kg) via tail vein, drug was allowed to circulate for 5 min, and mice were then sacrificed by CO₂ inhalation. Euthanized, *i.e.*, hypoxic, animals were maintained at 37°C for 1 h to allow binding of the drug that had perfused the tumor. Because viable tissue is necessary for drug bioreduction, this binding took place early in the 1-h incubation before metabolism ceased in the hypoxic tumor. Tumors were then frozen, sectioned, and stained for EF3 binding following the standard protocol (13). The time points of EF3 administration that were investigated included: control tumors (no PDT), immediately before beginning PDT at 75 mW/cm², 23 J/cm² (5 min of treatment), during the delivery of 45–68 J/cm² of 75 mW/cm² PDT (5 min), during the delivery of 45–57 J/cm² of 38 mW/cm² PDT (5 min), and 1.5 h after PDT at 75 mW/cm², 135 J/cm². The last time point was studied as a positive control for which EF3 access was expected to be limited because of delayed, PDT-associated vascular damage. In sections cut from these tumors, the evenness of EF3 binding was rated using the observed correlation in binding as a function

of inter-pixel distance. The spatial autocorrelation was calculated based on isotropic measurements and interpreted with the rationale that in a uniform surface the variability should reflect random noise with no correlation observed over long distances.

Statistical Analysis. All of the statistics were carried out with JMP (SAS Institute Inc., Cary, NC). The Wilcoxon rank-sum test was used to compare mean values for y_0 , a , and percentage of perfusion between controls and PDT-treated tumors. The t test was used to compare the median value for cell distance to a perfused blood vessel between controls and PDT-treated tumors. For both tests a $P < 0.05$ was considered significant.

RESULTS

EF3 Distribution in Euthanized (Hypoxic) Animals. Euthanized animal studies were used to investigate the effects of PDT treatment on EF3 delivery to and distribution in a tumor. Animals were administered EF3 at time points before, during, or after PDT. After a 5-min incubation to allow drug circulation, severe, tumor-wide hypoxia was created by euthanizing the animal, and EF3 binding was allowed to take place over the subsequent 60 min. The distribution of binding in frozen tumor sections was studied as an indication of drug access to that tumor. The evenness of EF3 binding was rated using the observed correlation in binding levels across the section. Fig. 1 demonstrates two representative patterns in the correlation. Fig. 1A is characterized by a rapid drop in the observed correlation to values of approximately zero. This lack of correlation is expected in sections with visually apparent, well-distributed EF3 binding because of the granular nature of binding. The plot of Fig. 1B represents a section with uneven EF3 binding, where after a short lag distance a negative relationship is found between the sampled EF3 intensities. In this section, an absence or severely limited amount of EF3 binding in some areas negatively correlated with substantial binding found >400 pixels away.

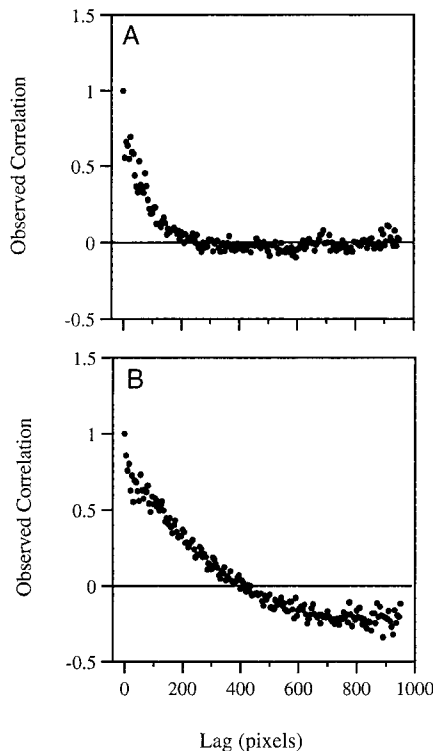


Fig. 1. Correlation in EF3 binding as a function of the lag distance between pixels sampled on an image. In euthanized animal studies, the correlation in EF3 binding levels was calculated to study EF3 access to tumors under different experimental conditions. The plot of A is representative of the observed correlation in an image of a tumor well perfused by EF3. The plot of B is representative of the correlation in an image with uneven EF3 binding because of poor drug access.

Table 1 EF3 access and distribution in PDT treated tumors^a

Time of EF3 administration	Sections with uneven binding/total	Degree of unevenness ^b
Control	1/7	+
75 mW/cm ²		
Immediately before PDT	1/5	+
During PDT	1/6	++
1.5 h after PDT	3/5	++
38 mW/cm ²		
During PDT	0/4	-

^a EF3 access was determined by studies in euthanized animals. In each treatment category, the number of sections demonstrating uneven binding is indicated. In the sections with uneven binding, the degree of nonuniformity is rated.

^b The evenness of binding was rated based on the shape of the EF3 correlation curve. A curve that formed a plateau at zero (Fig. 1A) was rated negative (-) or representative of even binding. Curves that showed some nonuniformity in EF3 binding were rated as positive. A + curve (minimal nonuniformity) fluctuated around a correlation of zero, but with a variability larger than that seen in Fig. 1A. A ++ curve (moderate nonuniformity) clearly demonstrated a negative correlation (Fig. 1B).

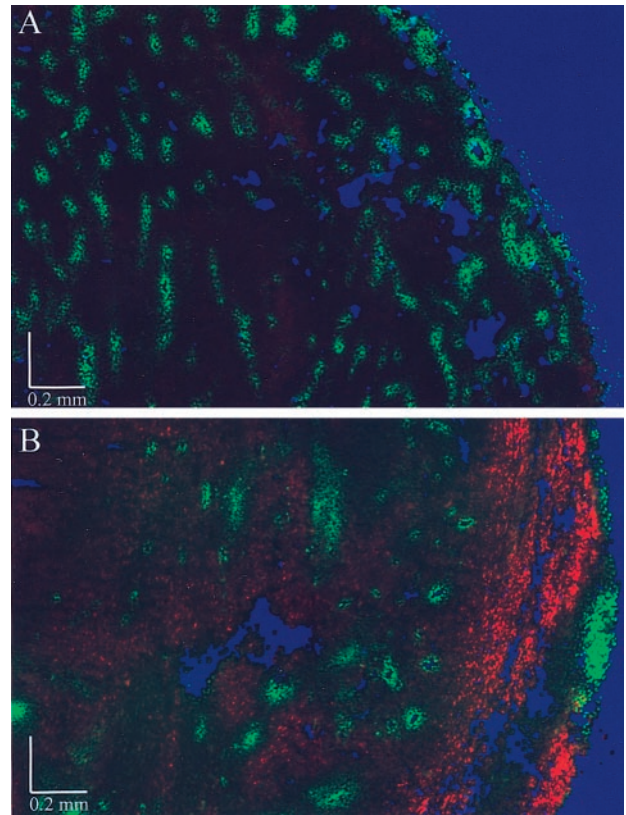


Fig. 2. EF3 binding (red) and vascular perfusion (green) in a control (A) and a PDT-treated (75 mW/cm², 135 J/cm²) tumor (B). For B, EF3 labeling took place during the PDT treatment itself. The level of binding, *i.e.*, the severity of hypoxia, is indicated by the red color intensity. To permit intratumoral discrimination of EF3 binding levels, color intensities are adjusted such that EF3 binding during PDT is 3 times that seen in the control. In actuality, however, binding during PDT was 20 times that found in the control. Perfusion was labeled by animal injection with Hoechst 33342 at 1.5 min before tumor excision. Tissue-containing areas were labeled by flooding the sections with a solution of Hoechst 33342 after other photography was completed; the inverse of Hoechst fluorescence, *i.e.*, nontissue areas, is shown in blue.

Table 1 summarizes the number of sections exhibiting poorly distributed EF3 and the severity of the unevenness in EF3 binding from tumors treated as controls or with PDT. Only 1 of the 5–7 sections studied per group demonstrated any nonuniformity in EF3 binding when the marker was administered to animals immediately before PDT (75 mW/cm²), during PDT (75 mW/cm²), or to untreated controls. In the 1 section per group, minimal nonuniformity was found in the controls and tumors exposed to EF3 before PDT. Moderate

nonuniformity was found in 1 section from an animal that received EF3 during PDT. In contrast, moderate nonuniformity in binding was found in the majority of tumor sections from animals that received EF3 at 1.5 h after the completion of PDT. This condition was evaluated as a positive control for which PDT-created vascular damage was expected to limit EF3 access to the tumor. No unevenness in EF3 binding was detected in tumor sections from animals that received EF3 during PDT at 38 mW/cm².

Intratumoral Distribution of Oxygen in Control and PDT-treated Tumors. The spatial distribution of hypoxia was studied in control RIF tumors and those exposed to EF3 during Photofrin-PDT at 75 mW/cm², 135 J/cm². Whereas only discrete regions of low-level EF3 binding (red) were found in control tumors (Fig. 2A), significant and widespread binding occurred during PDT (Fig. 2B). PDT-created hypoxia was found even in close proximity to blood vessels, as shown by EF3 binding in regions adjacent to perfused vessels (green). However, binding was visibly higher in vascular-remote areas. To quantify the distribution of hypoxia, image analysis was performed to characterize EF3 binding levels as a function of distance to the nearest perfused blood vessel.

For the purpose of image analysis, sections were divided into those collected from within the superficial 600 μm of the tumor (surface) or those collected from within 600 μm of the base of the tumor (deep). Fig. 3 plots the EF3 distribution in surface and deep sections from tumors receiving PDT at 75 mW/cm², 135 J/cm². For comparison, EF3 binding in representative controls, *i.e.*, marker and light, is shown as well. In the controls, a slight or no increase in EF3 binding was found with increasing distance to the nearest perfused blood vessel. In contrast, prominent gradients of increasing EF3 binding at increased distance to a perfused blood vessel were found in many of the

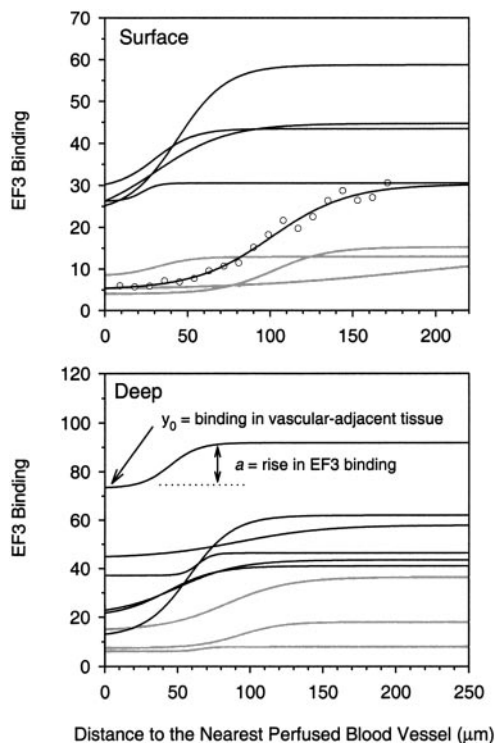


Fig. 3. The spatial distribution of EF3 binding relative to cell distance to the nearest perfused blood vessel. Sections were divided into those collected from the surface or deep sides of RIF tumors. Tumors exposed to EF3 during light-alone (75 mW/cm², 135 J/cm²) are shown in gray and tumors exposed to EF3 during Photofrin-PDT (75 mW/cm², 135 J/cm²) are shown in black. Curves were drawn based on a 4 parameter sigmoid curve fit to the data points. For clarity, the individual data points of only a representative plot (○) are depicted. On another representative plot, the “ y_0 ” and “ a ” values are indicated.

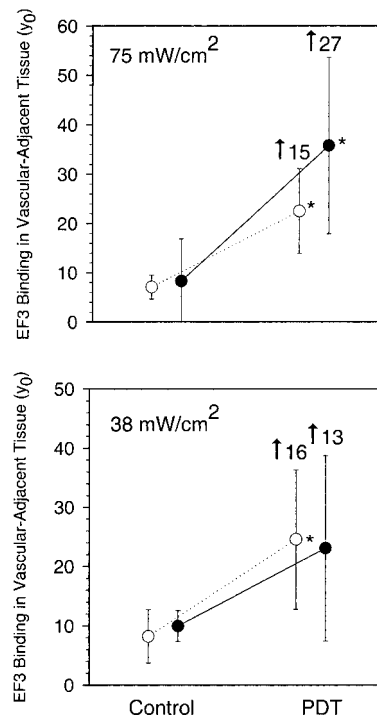


Fig. 4. EF3 binding in vascular-adjacent tissue (y_0) in controls and tumors treated with PDT at 75 or 38 mW/cm². Sections are divided into those collected from the surface (○) or deep (●) side of tumors, and each plot indicates the increase in y_0 that occurred during PDT. The number above each plot is the calculated increase in y_0 that resulted from PDT. * indicates that EF3 binding significantly increased during PDT when compared with controls. Each point depicts the mean \pm 95% CI. Five to nine tumors were included in each group.

PDT-treated tumors. The treated tumors clearly all demonstrated more severe hypoxia in vascular-distant tissue than that found in controls. Furthermore, in all but one of the PDT-treated tumors, EF3 binding in vascular-adjacent tissue was higher than that found in controls.

To evaluate the effects of fluence rate on oxygen gradients during PDT, additional studies were carried out with PDT delivered at 38 mW/cm², 135 J/cm², *i.e.*, a fluence rate half of the standard 75 mW/cm². As with the 75 mW/cm² fluence rate, EF3 labeling took place during the illumination period. Note, however, that illumination to a total fluence of 135 J/cm² required 60 min of treatment at 38 mW/cm² and 30 min of treatment at 75 mW/cm². For this reason, EF3 binding levels are not directly compared between tumors receiving 75 mW/cm² versus 38 mW/cm² illumination. Rather, tumors treated at each fluence rate are compared with their appropriate (timed-based) controls.

Fig. 4 plots the average EF3 binding in vascular-adjacent tissue for control tumors and those receiving PDT at 38 or 75 mW/cm². The level of EF3 binding in vascular-adjacent tissue was calculated as the y intercept (y_0) from the sigmoid curve fits shown in Fig. 3. In tumors receiving 75 mW/cm² PDT, a significant increase in y_0 was found in both the surface and deep sections. During PDT, y_0 increased >3 -fold in the surface sections and >4 -fold in the deep sections. The average PDT-induced increase in y_0 in the surface sections was 15 fluorescence intensity units and almost double this (27) in deep sections. In tumors receiving 38 mW/cm² illumination, y_0 increased ~ 3 -fold in surface sections. However, in the deep sections, an insignificant increase of only ~ 2 -fold was found to result from PDT.

Spatial gradients in hypoxia were quantified as the rise in EF3 binding that occurred as a function of increasing distance to the nearest perfused blood vessel. This rise, called a , is a parameter of the sigmoid curve fit. It is based on the increase in EF3 binding that

occurred between plateaus (see Fig. 3). PDT at 75 mW/cm² caused a significant increase in *a* in both surface and deep sections (Fig. 5). At the tumor surface, *a* was >4.5 times higher in treated tumors than in controls. In deep sections, the rise was almost 4-fold higher during PDT than in controls. As a consequence of PDT, *a* increased an average of 15 and 14 fluorescence intensity units, in surface and deep sections, respectively. During PDT at 38 mW/cm², *a* increased 4-fold in surface sections. However, in deep sections from these tumors, *a* insignificantly increased less than 2-fold.

Perfusion in Control and PDT-treated Tumors. The development of hypoxia during PDT can be attributed to oxygen consumption by PDT photochemistry as well as to limitations in oxygen delivery as a consequence of PDT-created damage to the tumor vascular network. Thus, gradients in hypoxia during illumination can result in part from impaired blood vessel function during PDT and associated increases in functional intervascular spacing. To study this phenomenon, sections from PDT-treated and control tumors were analyzed to determine distance from a cell to the nearest perfused blood vessel. Histograms of the average distance from a cell to the nearest perfused blood vessel are plotted in Fig. 6. In control tumors for 75 mW/cm² illumination, the median cell to blood vessel distance was 32.5 ± 3.5 (SE) μm and 27.3 ± 3.2 μm in surface and deep sections, respectively. During PDT at 75 mW/cm², the median distance increased significantly to 65.5 ± 13.9 μm (*P* = 0.009) in the surface sections and to 153.2 ± 66.7 μm (*P* = 0.026) in the deep sections. In tumors treated with PDT at 38 mW/cm², the median distance of a cell to the nearest perfused blood vessel did not differ significantly from controls. These distances were: control surface, 37.5 ± 9.3 μm; control deep, 38.0 ± 9.4 μm; PDT surface, 40.9 ± 3.8 μm; and PDT deep, 49.8 ± 10.8 μm.

To study PDT effects on blood vessel perfusion, the percentage of structurally identified (labeled by CD31staining) blood vessels, which

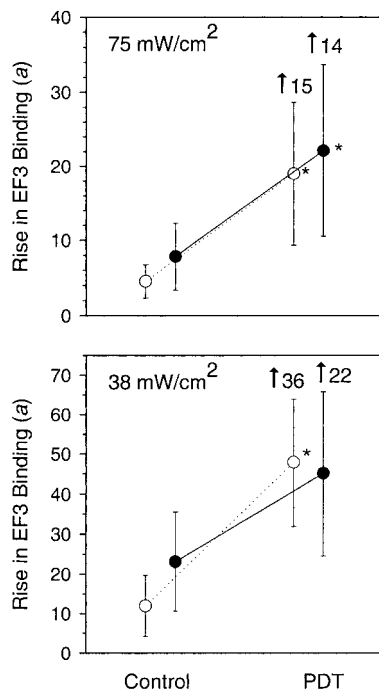


Fig. 5. The distant-dependent rise (*a*) in EF3 binding in controls and tumors treated with PDT at 75 or 38 mW/cm². Sections are divided into those collected from the surface (○) or deep (●) side of tumors, and each plot indicates the increase in *a* that occurred during PDT. The number above each plot is the calculated increase in *a* that resulted from PDT. * indicates that *a* significantly increased during PDT when compared with controls. Each point depicts the mean ±95% CI. Five to 9 tumors were included in each group.

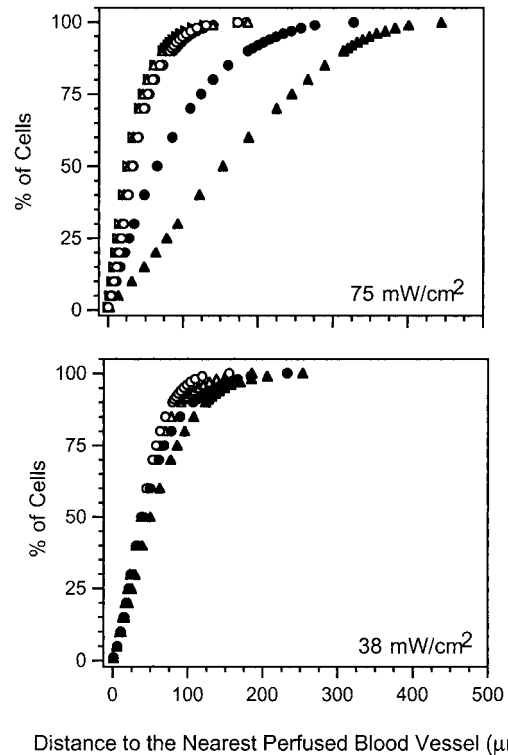


Fig. 6. Cell distance to the nearest perfused blood vessel during PDT at 75 mW/cm² or 38 mW/cm². Plots indicate the frequency distribution of the average distance from a cell to the nearest perfused blood vessel. Symbols indicate sections from the surface, control (○); surface, PDT-treated (●); deep, control (△); and deep, PDT-treated (▲). Five to 9 tumors were included in each group.

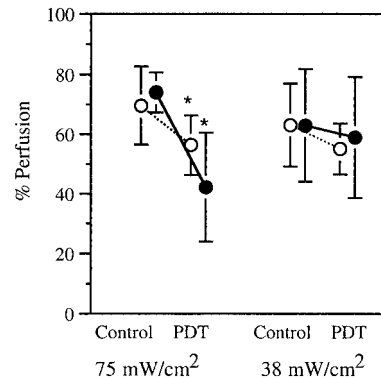


Fig. 7. The perfused percentage of blood vessels in tumors receiving PDT at 75 mW/cm² or 38 mW/cm². Sections are divided into those collected from the surface (○) or deep (●) side of tumors, and each plot indicates the change in perfusion that occurred during PDT. * indicates that perfusion significantly decreased during PDT when compared with controls. Each point depicts the mean ±95% CI. Five to 9 tumors were included in each group.

were perfused (labeled by i.v.-injected Hoechst dye), was determined (Fig. 7). During PDT at 75 mW/cm², the perfused percentage of blood vessels dropped significantly from 70% to 56% in surface sections and from 74% to 42% in deep sections. During PDT at 38 mW/cm², insignificant changes in the perfused percentage of blood vessels were found. In both surface and deep sections, controls exhibited a perfused percentage of 63%. A minor decrease to 55% in surface sections and to 59% in deep sections was found during PDT.

DISCUSSION

Using the hypoxia marker EF3, we have quantified the intratumoral, microscopic, spatial distribution of oxygen during PDT of RIF

tumors. Fluence rate-dependent effects on oxygen gradients were apparent. A low fluence rate of 38 mW/cm² caused only nonsignificant increases in hypoxia in vascular-adjacent tissue (y_0) in deep sections, whereas a fluence rate of 75 mW/cm² resulted in significant oxygen depletion in vascular-adjacent tissue and a significant increase in the distant-dependent rise in hypoxia (a), regardless of tumor depth. Contributing to hypoxia during PDT at 75 mW/cm² was a reduction in tumor perfusion that occurred during light treatment. The median distance from a cell to the nearest perfused blood vessel significantly increased in both surface and deep sections of 75 mW/cm²-treated tumors. Conversely, during PDT at 38 mW/cm², no effect of PDT on the median distance from a cell to a perfused vessel or on the perfused percentage of blood vessels was detected. Thus, the significant increases in y_0 and a found at the surface of 38 mW/cm²-treated tumors and the insignificant increases found at deeper depths are likely a consequence of photochemically induced oxygen depletion. This conclusion is additionally supported by the observation that, as found with 38 mW/cm² PDT, photochemical oxygen depletion would be expected to have a decreasing effect with increasing tumor depth because of the attenuation of the activating light.

Although this is the first imaging technique described to quantify microscopic radial gradients in oxygen during PDT, studies by others have suggested the presence of such gradients. Pogue *et al.* (7) recently described significant heterogeneity in the electrode-measured oxygenation of rodent tumors during verteporfin PDT. Similarly, the data of Curnow *et al.* (8) demonstrate differing profiles of oxygen depletion from electrode measurements made at separate tumor locations during PDT. In studies by van Geel *et al.* (12), which used the hypoxia marker NITP, an inverse relationship was observed between hypoxia and vascular perfusion in tumors studied after PDT. Mathematical modeling based on the measured oxygen consumption in PDT-treated spheroids by Nichols and Foster (16) predicted a fluence-rate dependence to oxygen gradients formed during PDT. Correspondingly, in tumors *in vivo*, fluence rate effects on PDT-created oxygen depletion were found (6).

Lower PDT fluence rates favor the development of delayed but response-contributing vascular damage (17). The present data suggest that delayed damage may occur, in part, as a consequence of better oxygen maintenance in vascular-adjacent tissue during low fluence rate PDT. In contrast, during PDT at a higher fluence rate, perivascular hypoxia developed during the treatment. This hypoxia would be expected to be inconsequential if PDT-created reductions in tumor perfusion are long lasting and ultimately contribute to tumor response. On the other hand, reversible changes in tumor perfusion, as have been found by others (18), would suggest that the perivascular hypoxia is therapy limiting. Ongoing studies will apply this new image analysis technique to address the spatial association between PDT-created hypoxia and tumor damage.

In using EF3 to label hypoxia during tumor exposure to a perfusion-modifying condition, such as PDT, appropriate control studies must be performed to ensure that the vascular delivered drug adequately perfuses the tissue of interest. These controls, called euthanized animal studies, evaluate the uniformity of EF3 binding in tumors in which the drug was permitted to distribute for 5 min and then binding was facilitated by severe (uniform) hypoxia. The distribution of drug binding in sections cut from these tumors is an indication of EF3 perfusion of the tumor. These studies demonstrate that EF3 access to tumors during PDT (for marker administered either immediately before or during the treatment) was similar to that found in controls. Only 0–1 sections per treatment group exhibited any unevenness in EF3 binding. In comparison, when EF3 was administered at a delayed time point (1.5 h) after PDT, the majority of the sections demonstrated uneven binding as expected because severe post-therapy vascular

damage would limit EF3 delivery. The uneven binding found in the 0–1 sections in the former groups may reflect, in part, the limitations of the methods being used. For example, our interpretation of the correlation values assumes that any unevenness in the brightness of the photographed tissue is a consequence of limitations in drug distribution. In actuality, however, small inconsistencies in image brightness may result from minor nonuniformity in the illumination field. The presence of scattered nonviable cells within tumors will cause some inherent nonuniformity in binding, because viable tissue is necessary for bio-reduction of the drug. Furthermore, in studies evaluating EF3 access during PDT, the nonuniform hypoxia created by PDT itself will cause binding to take place during the 5 min that drug is allowed to circulate before animal euthanasia. Although the short 5-min drug circulation time was chosen to try to minimize this effect, we cannot rule out that outcome-affecting levels of binding may have occurred in areas made severely hypoxic by PDT. Ultimately, however, the adequate distribution of EF3 during PDT treatment is evidenced by the fact that at least low levels of EF3 binding can be visualized throughout PDT-treated tumors as depicted in Fig. 2B. Sufficient distribution of EF3, despite decreases in blood vessel perfusion, is possible because of the long diffusion distance of hypoxia markers.

Also to be considered in relation to the methodology used for this study is the absence of hypoxia gradients as a function of distance to a blood vessel in the control tumors. Several factors likely contribute to this finding. RIF tumors are known to be well vascularized and exhibit a small radiobiologically determined hypoxic fraction (19), so small, metabolically created gradients in oxygen would be expected to exist. However, it is important to note that the hypoxia marker incubation times in controls were relatively short (30 or 60 min) to match the time of EF3 incubation during PDT. Because EF3 binding is time dependent as well as oxygen dependent, short incubation times in well-oxygenated tumors lead to lower signals. It is because of the minimum to low binding that occurs in the controls that the 1-h controls do not exhibit binding levels that are twice that found in the 30 min controls, but, as expected, some spread in these values is visible (*e.g.*, see Fig. 5). Importantly, under conditions of moderate to extreme hypoxia, a 30-min incubation time is sufficient to cause substantial hypoxia labeling, as indicated by the significant increases in EF3 binding during 30 min of PDT.

In conclusion, the significance of image analysis for quantification of oxygen distribution during PDT lies in the use of such techniques to assess the relationship between treatment-created oxygen gradients and subsequent damage development. For example, the presence of significant hypoxia in vascular-adjacent tissue during PDT at 75 mW/cm² indicates that oxygen depletion during PDT can extend to even perivascular areas. Ongoing studies evaluate the association of regional oxygen depletion or maintenance with the development of sustained, response-contributing blood vessel damage. These data may ultimately be used in the development of monitoring or dosimetry instrumentation to individually optimize PDT treatment.

ACKNOWLEDGMENTS

We thank Jeremy Miles for assistance with the laser and W. Timothy Jenkins for helpful conversations.

REFERENCES

1. Moan, J., and Sommer, S. Oxygen dependence of the photosensitizing effect of hematoporphyrin derivative in NHIK 3025 cells. *Cancer Res.*, 45: 1608–1610, 1985.
2. Chapman, J. D., Stobbe, C. C., Arnfield, M. R., Santus, R., Lee, J., and McPhee, M. S. Oxygen dependency of tumor cell killing *in vitro* by light-activated Photofrin II. *Radiat. Res.*, 126: 73–79, 1991.

3. Foster, T. H., Murant, R. S., Bryant, R. G., Knox, R. S., Gibson, S. L., and Hilf, R. Oxygen consumption and diffusion effects in photodynamic therapy. *Radiat. Res.*, *126*: 296–303, 1991.
4. Wieman, T. J., Mang, T. S., Fingar, V. H., Hill, T. G., Reed, M. W., Corey, T. S., Nguyen, V. Q., and Render, E. R., Jr. Effect of photodynamic therapy on blood flow in normal and tumor vessels. *Surgery (St. Louis)*, *104*: 512–517, 1988.
5. Fingar, V. H., Wieman, T. J., Park, Y. J., and Henderson, B. W. Implications of a pre-existing tumor hypoxic fraction on photodynamic therapy. *J. Surg. Res.*, *53*: 524–528, 1992.
6. Sitnik, T. M., Hampton, J. A., and Henderson, B. W. Reduction of tumour oxygenation during and after photodynamic therapy *in vivo*: effects of fluence rate. *Br. J. Cancer*, *77*: 1386–1394, 1998.
7. Pogue, B. W., Braun, R. D., Lanzen, J. L., Erickson, C., and Dewhirst, M. W. Analysis of the heterogeneity of pO₂ dynamics during photodynamic therapy with verteporfin. *Photochem. Photobiol.*, *74*: 700–706, 2001.
8. Curnow, A., Haller, J. C., and Bown, S. G. Oxygen monitoring during 5-aminolaevulinic acid induced photodynamic therapy in normal rat colon. Comparison of continuous and fractionated light regimes. *J. Photochem. Photobiol. B*, *58*: 149–155, 2000.
9. Dewhirst, M. W., Secomb, T. W., Ong, E. T., Hsu, R., and Gross, J. F. Determination of local oxygen consumption rates in tumors. *Cancer Res.*, *54*: 3333–3336, 1994.
10. Helmlinger, G., Yuan, F., Dellian, M., and Jain, R. K. Interstitial pH and pO₂ gradients in solid tumors *in vivo*: high-resolution measurements reveal a lack of correlation. *Nat. Med.*, *3*: 177–182, 1997.
11. Henning, J. P., Fournier, R. L., and Hampton, J. A. A transient mathematical model of oxygen depletion during photodynamic therapy. *Radiat. Res.*, *142*: 221–226, 1995.
12. van Geel, I. P., Oppelaar, H., Rijken, P. F., Bernsen, H. J., Hagemeyer, N. E., van der Kogel, A. J., Hodgkiss, R. J., and Stewart, F. A. Vascular perfusion and hypoxic areas in RIF-1 tumours after photodynamic therapy. *Br. J. Cancer*, *73*: 288–293, 1996.
13. Busch, T. M., Hahn, S. M., Evans, S. M., and Koch, C. J. Depletion of tumor oxygenation during photodynamic therapy: detection by the hypoxia marker EF3 [2-(2-nitroimidazol-1-[H]-yl)-N-(3, 3, 3-trifluoropropyl)acetamide]. *Cancer Res.*, *60*: 2636–2642, 2000.
14. Evans, S. M., Hahn, S., Pook, D. R., Jenkins, W. T., Chalian, A. A., Zhang, P., Stevens, C., Weber, R., Weinstein, G., Benjamin, I., Mirza, N., Morgan, M., Rubin, S., McKenna, W. G., Lord, E. M., and Koch, C. J. Detection of hypoxia in human squamous cell carcinoma by EF5 binding. *Cancer Res.*, *60*: 2018–2024, 2000.
15. Busch, T. M., Wileyto, E. P., Evans, S. M., and Koch, C. J. Quantitative spatial analysis of hypoxia and vascular perfusion in tumor sections. *Adv. Exp. Med. Biol.*, in press, 2003.
16. Nichols, M. G., and Foster, T. H. Oxygen diffusion and reaction kinetics in the photodynamic therapy of multicell tumour spheroids. *Phys. Med. Biol.*, *39*: 2161–2181, 1994.
17. Henderson, B. W., Sitnik-Busch, T. M., and Vaughan, L. A. Potentiation of PDT anti-tumor activity in mice by nitric oxide synthase inhibition is fluence rate dependent. *Photochem. Photobiol.*, *70*: 64–71, 1999.
18. Fingar, V. H., Wieman, T. J., Wiehle, S. A., and Cerrito, P. B. The role of microvascular damage in photodynamic therapy: the effect of treatment on vessel constriction, permeability, and leukocyte adhesion. *Cancer Res.*, *52*: 4914–4921, 1992.
19. Henderson, B. W., and Fingar, V. H. Oxygen limitation of direct tumor cell kill during photodynamic treatment of a murine tumor model. *Photochem. Photobiol.*, *49*: 299–304, 1989.